Implications of Runway Direction Changes for improved Arrival Management at Singapore Changi Airport

Ehsan Asadi[1], Gabriele Enea[2], Sameer Alam[3], Michael Schultz[1],

[1] Institute of Flight Systems, University of the Bundeswehr Munich, Germany
[2] ATC & Weather Systems Group, MIT Lincoln Laboratory, Lexington, USA
[3] Air Traffic Management Research Institute, School of Mechanical and Aerospace Engineering
Nanyang Technological University, 637460, Singapore

***Abstract*—This paper develops a runway-aware approach to improve the arrival management Singapore Changi (WSSS), where frequent weather-driven operating-direction changes cause time-varying airport capacity. Using Meteorological Aerodrome Report (METAR)-derived Air Traffic Management Advancement Program (ATMAP) scores, track-based direction detection, and rolling-hour sector-entry counts at a 170-NM reference ring, we first establish a stable baseline (5–20 Sep 2019, predominantly North operations) to construct a standardized capacity template. The effect of runway direction changes (flips) is then characterized via a compact parameterization: a small pre-flip capacity overshoot, a post-flip capacity trough, and followed by a brief capacity compensation bump. On a flip-rich day (25 Sep 2019, ten direction changes), the reduction in throughput begins 10–15 min before a change; early-morning flips produce deficits of -8 to -15 movements/h for 45–60 min (up to 90 min when flips cluster), while mid-morning effects are milder (-3 to -6/h for 30–45 min). Embedding this piecewise envelope in a metering optimization with Long Range Air Traffic Flow Management (LR-ATFM)-feasible time-shift options, we reduce the integral of overload from 2085 to 395 flight-minutes (-81%), with the maximum residual exceedance limited to 6 aircraft during the deepest morning trough. Results show that modest, upstream time adjustments aligned to runway-aware capacity trajectories can materially mitigate overloads without aggressive tactical intervention, providing an effective pre-condition of the flow for the Arrival Manager (AMAN).**

***Keywords*—Air Traffic Flow Management; Arrival Management; Airport Operations; Airport Capacity Optimization; Weather Impact**

I. Introduction

Demand–capacity balancing remains a central challenge in the Asia-Pacific (APAC) air transportation system, where heterogeneous regional Air Traffic Flow Management (ATFM) implementations meet dense long-haul traffic at major hubs [1]. Singapore Changi (WSSS) is a key node in this network, serving more than 100 airlines and connecting to 300+ cities, with three parallel runways and continuous operations. In this environment, local arrival performance is sensitive to constraints that vary across the day and across seasons, which necessitates planning approaches that look beyond the terminal area and anticipate inbound flows far upstream (cf. [2]).

Long Range Air Traffic Flow Management (LR-ATFM) extends conventional ATFM by issuing Target Times Over (TTO) reference points well before top-of-descent and by enabling moderate in-cruise speed advisories coordinated with airline operations centers [3]. The concept is organized around a five-step workflow that establishes an Estimated Time Over, computes and communicates a TTO at a chosen metering fix, secures flight crew acknowledgment, and manages conformance or revisions as needed. For WSSS, the transition from LR-ATFM to local arrival management is set at a TTO reference distance of about 170 NM, reflecting where most flights initiate descent and where terminal area procedures in some part of the world take over. Trials and modeling show that only salient speed changes should be advised (e.g., more than 0.01 Mach), both to limit cockpit workload and to preserve acceptance.

The composition and timing of WSSS arrivals provide the operational lever for LR-ATFM. Differently from other international hubs, more than 50% of inbound flights have flight times longer than three hours [4], and approximately 25% qualify as long-haul (>2,200 NM) [5]. Inbound flows merge from nine dominant bearings, and recurrent afternoon peaks arise when long-haul streams coincide with short-/medium-haul banks. A sensible approach to assess approach-sector capacity is to count hourly entries and use the 90th percentile as the planning value [6]; in the operational scenarios this corresponds to a capacity on the order of 20 to 30 movements per rolling hour at the sector entry. Within this framing, LR-ATFM regulates entry times to the 170 NM reference by small, cumulative speed adjustments that exploit remaining cruise time while aiming to arrive at the terminal area with little or no tactical re-sequencing.

In optimization studies for WSSS that treat long-haul arrival times as normal-distributed and shiftable by bounded per-hour adjustments, the integral of over-demand (the area where the demand exceeds the capacity line) can be reduced by 14% with ± 1 min per flight hour and by up to 80% with ± 6 min per hour, underlining the sensitivity of the peak to modest upstream actions [7]. Complementary agent-based simulations that couple LR-ATFM with local arrival management report at least a 26% reduction in the number and duration of holdings in the test case, demonstrating operational relevance

when upstream control is integrated with the terminal-area sequence. At the same time, route-specific procedures also have an impact: APAC flight trials between New Zealand and Singapore observed that achievable time absorption differed by direction and infrastructure, with about 2–3 minutes per hour in one direction versus about 1 minute per hour in the Singapore-bound direction, reflecting Flight Information Regions (FIRs) structure and traffic load.

With this premise, WSSS flows from Australia and New Zealand are a natural focus for LR-ATFM because they form a coherent southeastern inbound stream in the clustered arrival network and provide extended cruise segments for controlled adjustments before the 170 NM reference point. Building on the published concept and implementation results, this paper targets the pre-tactical integration of these southern flows into WSSS arrival planning.

For LR-ATFM, effective arrival planning hinges on credible, time-indexed knowledge of the destination airport's usable arrival capacity. At WSSS, weather-driven changes in operating direction imprint a significant and characteristic signature on throughput. In this paper, we infer those capacity dynamics from flow observations—rolling-hour sector-entry counts, near-field tracks for direction detection, and Meteorological Aerodrome Report (METAR)/Air Traffic Management Advancement Program (ATMAP) weather signals—and summarize them in a compact, runway-aware capacity model for inbound arrival management. We use this model to frame the metering problem addressed here, and we see it as the foundation for a subsequent extension of our LR-ATFM approach with an explicit focus on incoming traffic flows.

The objectives are to (i) partition long-haul demand into direction-based sub-flows aligned with observed clustering, (ii) apply empirically grounded, direction-specific bounds on feasible time targets consistent with APAC trials, and (iii) quantify the impact on approach sector over demand and terminal area holdings under capacity values derived from observed hourly entries. Therefore, this paper aims to:

- prepare dataset from actual situation at WSSS;
- model inbound flows;
- optimize arrival times at WSSS airport (rough benefit evaluation from WSSS view);
- check the feasibility of the solutions (time shift in arrival);
- evaluation of benefit per flight.

II. Runway Change at WSSS and Weather Drivers

Runway configuration changes at WSSS are not rare edge cases but a recurring operational problem with measurable impact on arrival performance. Because the two civil runways (02L/20R and 02C/20C) are aligned roughly along the 020°/200° axis and because the local wind regime is strongly seasonal, the airport alternates between *North* (runway designator 02, arrivals from the South) and *South* (runway designator 20, arrivals from the North) operations [8].

A runway change is the discrete switch between these two airport operating directions.[1] While each single change is short in clock time, the system wide ripple is not negligible: sequences must be re-built, approach spacing gets temporarily conservative, and departure queues re-ordered. In our data, a change is usually followed by a short, but visible dip in movements (arrivals and departures) [9].

A. Why runway changes matter for arrivals

Arrival management at WSSS relies on a stable operating direction, since vectoring and merge points in the terminal area are designed around it [10]. When the direction flips, otherwise orderly arrival streams—often structured around long-haul banks from Australia/New Zealand and medium-haul banks from Association of Southeast Asian Nations (ASEAN)—must be re-phased [11]. Even with efficient ATC, the combined effects of (i) switching to a new preferred Standard Terminal Arrival Route (STAR), (ii) short-term sector re-balancing, and (iii) additional pilot workload for new approach in communications between ATC and landing flights introduce additional delays and inefficiencies [12]. These small delays add up, resulting in modest but noticeable reductions in rolling-hour entry counts and, more importantly, greater variability. From an LR-ATFM perspective, this variability is the key issue: even if the average traffic flow remains within limits, higher variance increases the risk that the movements will exceed capacity thresholds—precisely the conditions under which holdings begin to occur [13].

B. Primary meteorological triggers

The immediate trigger for a direction change at WSSS is the wind component on the runway axis [14]. Pilots and ATC avoid tailwind on final; if the actual tailwind rises beyond a small limit (practically on the order of a few knots; in this research notes we use 5–6 kt as a soft threshold), the configuration is switched from South to North or vice versa [15]. Moreover, two other tactical weather features affect WSSS operations:

- **Convective cells and storm lines** (e.g., Sumatra squalls). They produce abrupt shifts in surface wind direction and gusts, which can force a rapid turn of the preferred runway, sometimes twice within a short window. During the inter-monsoon periods, these cases are more frequent [16].
- **Micro-scale variability around showers.** Localized convection over the straits or the island often produces brief cross-/tail-wind surges on one runway end; in our data these episodes appear as ATMAP danger spikes (from the METAR-derived scoring) and correlate with quick direction flips and short throughput dips. In this paper, we use the EUROCONTROL ATMAP procedure to convert routine METAR reports into a time series of weather-impact scores for an aerodrome. ATMAP is not

[1]The third runway 02R/20L is used by Republic of Singapore Air Force (RSAF) and is not considered in the civil arrival capacity analysis.

an operational regulation; it is a rule-based diagnostic that flags conditions known to depress runway throughput [17]. Five component scores are produced—Visibility, Wind, Precipitation, Freezing, and a composite Danger index—by mapping METAR elements (e.g., prevailing/lowest visibility, gusts and runway-aligned wind components, present weather codes such as TS/SH/RA, temperature/icing flags) to normalized severities (none → severe). We compute ATMAP at 5-min resolution and then apply a short weighted moving average and a rolling 60-min mean to align with our capacity windows. In the figures below, "ATMAP danger spikes" mark short episodes of convective or gusty weather that frequently coincide with runway-direction flips and short-lived capacity drawdowns.

In both patterns, the tower reacts for safety first. The cost is a transient loss of sequence optimality [18].

C. Seasonal background: monsoon regimes

Behind the tactical triggers sits a clear seasonal structure. The *Northeast Monsoon* (Dec–early Mar) brings more persistent northerly to northeasterly winds near the surface, favoring *South operations* (arrivals from the North, runway 20). The *Southwest Monsoon* (Jun–Sep) shifts the background flow to southwesterly and southerly, favoring *North operations* (arrivals from the South, runway 02). The two inter-monsoon periods (Mar–May and Oct–Nov) are more convectively active and less directional, i.e., more variable. In our wind rose analyses, this appears as broader lobes and greater scatter, while in operations, it is reflected in more frequent intra-day wind direction changes. In essence, the monsoon establishes the prevailing bias, whereas the inter-monsoon contributes to the variability or "noise" [19, 20]. This data analysis is discussed further in III.

D. Site, Weather, Data and Empirical Patterns (2018–2020)

Airport and layout: WSSS lies at the island's eastern tip and has been in operation since 1981 [21]. The airport has two civil parallel runways, each 4000 m × 60 m, spaced 1.64 km apart. This orientation supports parallel operations and reflects prevailing monsoon wind directions [22]. A third runway (2748 m), is located 1.8 km east of second runway (02C/20C) and is operated by the RSAF [22]. Changi serves more than 100 airlines flying to over 170 destinations in 50 countries. In 2024, it handled 67.7 million passengers, around 366,000 movements, 2 million tonnes of cargo, and about 7200 weekly flight [23, 24]. Long-term planning includes Terminal 5 and a fourth runway, raising capacity to around 135 million passengers annually [21].

Weather regime and operational relevance: Located near 1° N, WSSS experiences a tropical maritime climate with 2500 mm of mean annual rainfall [24, 25]. Rainfall gradients make the east (airport) generally drier than central and western Singapore. Temperatures remain stable year-round (31–33 ° C daytime; 23–25 ° C nighttime), so icing is not operationally relevant.

The wind regime follows four characteristic periods over the year [24–27]:

- Northeast monsoon (Dec–early Mar): wetter, stronger rainfall, N/NE winds
- Inter-monsoon I (late Mar–May): convectively active, highly variable
- Southwest monsoon (Jun–Sep): drier, with SW/S winds
- Inter-monsoon II (Oct–Nov): convectively active, variable

Singapore records over 100 thunderstorm days each year [24]. Sumatra squalls—organized convective lines moving from Sumatra across the Malacca Strait—occur mainly in the early morning during the southwest monsoon. They bring gusts of around 40–80 km/h, last 1–2 h, and often trigger rapid surface wind shifts, sometimes requiring runway direction changes [24, 25].

ATFM/Arrival Manager (AMAN) context (APAC): ATFM balances demand and capacity to prevent sector or airport overloads, thereby reducing delays and holding [28]. Implementation in the APAC region is context-specific; Singapore runs flow programs via a dedicated Air Traffic Flow Management Unit (ATFMU), including Calculated Take-Off Time (CTOT) issuance, minimum departure spacing, and slot regulations [29]. LR-ATFM extends the horizon by coordinating TTO across FIRs, while the terminal-area AMAN sequences inbound flights at thresholds or entry fixes, supporting predictable, low-noise, low-emission profiles [30, 31]. Our LR-ATFM concept links to AMAN at ∼170 NM TTO, near typical top-of-descent (cf. concept section above).

III. Data sets and pre-processing

In this paper, we draw on four data sources:

- METAR from airport weather station (wind, visibility, phenomena, etc.);
- ATMAP scores (visibility, wind, precipitation, freeze, danger) using the airport performance weather algorithm [17];
- Flight tracks with latitude, longitude, altitude, groundspeed, timestamp;
- Operational time stamps: Scheduled Time of Departure (STD), Scheduled Time of Arrival (STA), Actual Time of Departure (ATD), Actual Time of Arrival (ATA).

Weather time-series representation: We resample ATMAP to a uniform grid with step size $\Delta t = 5\,\text{min}$. To suppress spikes while preserving the diurnal structure, we apply a symmetric *5-sample* (25 min) weighted moving average with weights $[0.5, 1, 1, 1, 0.5]$ (normalized by $Z = 4$), followed by a centered rolling one-hour mean ($\pm 30\,\text{min}$); see Eq. 1 and the green line in Figure 3. This two-stage smoothing retains salient peaks (e.g., the 06:30 maximum on 20 Apr 2019) while avoiding over-smoothing of flip-related transients. The green line in Figure 3 plots the ATMAP "danger" component for 19 Apr 2019 as a function of local time (x-axis) with a unitless risk score (y-axis; higher = more adverse).

$$\hat{x}_t = \frac{1}{Z} \sum_{k=-n}^{n} w_k \, x_{t+k},$$
$$w_k = \begin{cases} \alpha, & |k| = n, \\ 1, & |k| < n, \end{cases}$$
$$Z = \sum_{k=-n}^{n} w_k. \tag{1}$$

Implementation details: we use $n = 2$ (5 points $\Rightarrow$ 25 min span), $\alpha = 0.5$, $\Delta t = 5$ min, hence $Z = 0.5+1+1+1+0.5 = 4$.

Wind roses and directional scoring: Using METAR wind data, we generate monthly wind roses (direction × speed; see Figure 1) and ATMAP-on-rose views, which project total or component scores into the same polar bins. Two data issues are addressed using ATMAP, variable wind bins are excluded, and its values are filtered out before plotting.

Traffic time-series and "rolling hour": To characterize traffic intensity, we count arrivals and departures in a rolling hour, updated every 5 min ($\pm 30/60/90/120$ min variants; see blue and orange lines in Figure 3). Typical days show high throughput between 05:00–18:00, followed by a routine evening trough, and an anti-phase pattern at night (more departures than arrivals around midnight). Geographic position maps one hour before landing reveal spatial funnels (the progressive narrowing of inbound trajectories into a few corridor-like paths as aircraft converge on WSSS) and typical approach distances ($\sim$650 km; 97th percentile), with strong southern flows in some windows.

Detecting operating direction from tracks: Using low-altitude track points (<4000 ft and <50 km from the airport), we classify each sliding window as North, South, Mixed, or No data. This approach avoids heading ambiguity and reduces misclassification from far-field traffic. The method captures both day- and month-level patterns, including the annual progression in 2019 (Figure 2 for April, June, and September 2019).

Coupling weather, traffic and direction: Joint plots illustrate how ATMAP peaks, direction flips, and rolling-hour traffic counts interact. On 15 Apr 2019, for example, a rise in ATMAP between 08:00–09:00 coincides with a North→South switch and a temporary dip in both arrivals and departures (Figure 3). Furthermore, a weekly series (Tuesdays in Aug 2019) shows mostly schedule-driven regularity. In contrast, pandemic-era traffic on 20 Apr 2020 shows extremely low counts (maximum 4 departures / 3 arrivals per rolling hour), unaffected by weather, serving as a counterfactual baseline (a reference day that approximates what operations would look like if the usual confounders were absent).

IV. Implications for LR-ATFM at WSSS

Classical LR-ATFM formulations regulate inbound demand against a fixed approach-sector ceiling; the situation at WSSS shows this premise is too coarse. Capacity at Changi behaves like a living envelope that tightens and relaxes with weather-driven operating-direction changes. Three empirical strands make the case. First, the seasonal wind regime establishes a directional bias (NE monsoon on South ops; SW monsoon on North ops), while inter-monsoon convection injects timing variability (Sumatra squalls, gust fronts). This pattern is visible in the wind roses views, where broader lobes and ATMAP-danger dominance coincide with the transitional months. Second, at the tactical scale, direction flips are followed by short, measurable throughput dips: on days with a flip, both arrivals and departures fall for $\sim$30–90 minutes as sectors, STAR usage, and crews reconfigure (Figure 3); conversely, during stable-direction days the rolling counts remain near their plateau except for the routine evening trough. Third, over longer windows the airport's typical high-utilization state sits around 20–30 movements per rolling hour in each stream, yet that "main cloud" masks transient drawdowns clustered near flip times. In effect, capacity at the 170 NM reference is not a constant; it is a time-indexed trajectory conditioned on runway direction and its transitions. For LR-ATFM, pushing demand toward a static ceiling risks stacking traffic against a temporarily weakened system; pushing it against a runway-aware envelope allows the regulator to anticipate the bottleneck and steer banks around them. The remainder of this section therefore reframes capacity as a direction-contingent, piecewise curve inferred from operations and weather: stable plateaus when the runway holds, calibrated depressions around observed flip windows, and a diurnal baseline that captures the routine evening reduction.

A. Reference capacity

To calibrate a runway-aware capacity envelope we first establish a baseline period that is essentially free of operating-direction flips. 5–20 September 2019 satisfies this requirement, where the airport ran almost continuously in North operations, with only isolated one-bin slivers marked as "Mixed". The direction timeline spans the interval, before the pattern becomes highly variable after 22 September when frequent North to South transitions appear. Using this stable block has two methodological benefits. First, it decouples capacity estimation from the short, post-flip drawdowns documented earlier, so the baseline reflects what the system can sustain when vectoring geometry, STAR usage, and crew procedures are held constant. Second, it fixes the operating direction in a meteorologically coherent regime (late Southwest-monsoon), thereby removing the seasonal bias highlighted in the wind-rose and ATMAP analyses (cf. Figure 1).

We construct a direction-specific reference curve $U_{\mathrm{ref}}^{\mathrm{N}}(t)$ at the 170 NM TTO ring as follows. For each local time stamp t (5-min cadence), we compute rolling-hour entry counts of inbound flights crossing the 170 NM boundary on every day in 5–20 September. Aggregating across these days, we take the 90th percentile of the distribution at each time t as the planning value, which captures the sustained plateau while filtering occasional schedule troughs. A light, zero-phase moving average preserves diurnal shape without

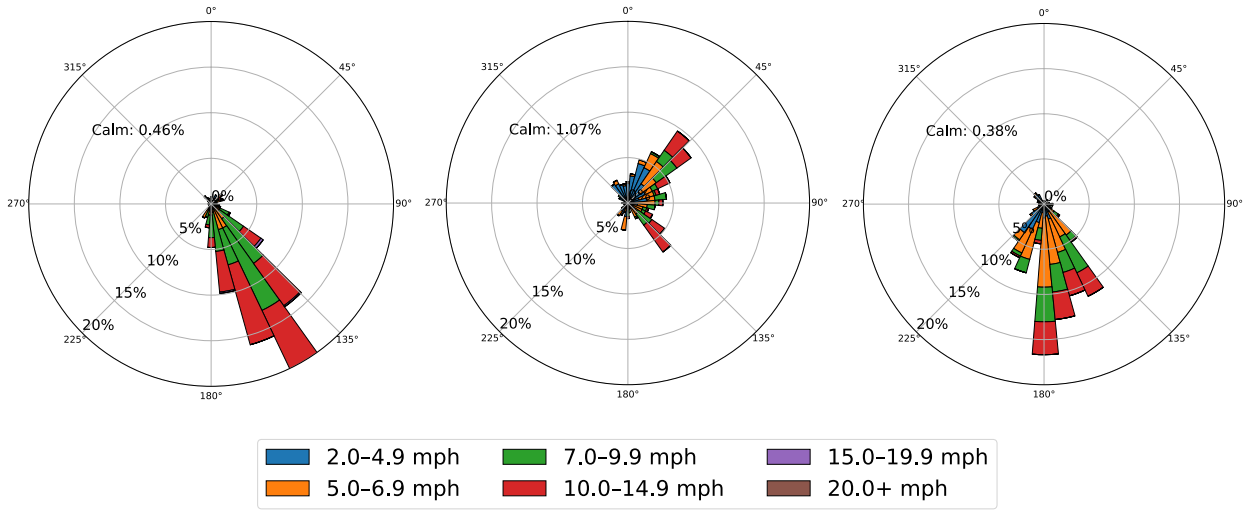

Figure 1. Windroses at Singapore Airport, showing the wind direction and wind speed for April, June, and September (from left to right).

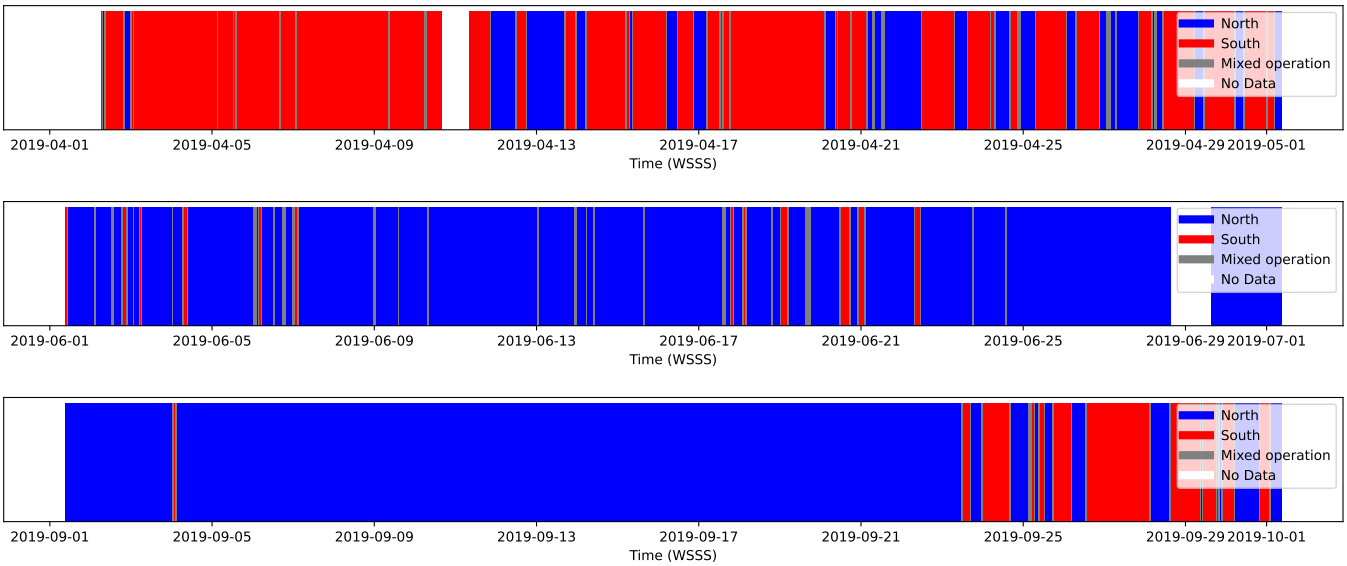

Figure 2. Operating direction of Singapore Airport for April, June, September (from top), showing the direction of the runway, blue for north, red for south, and gray for mixed operation.

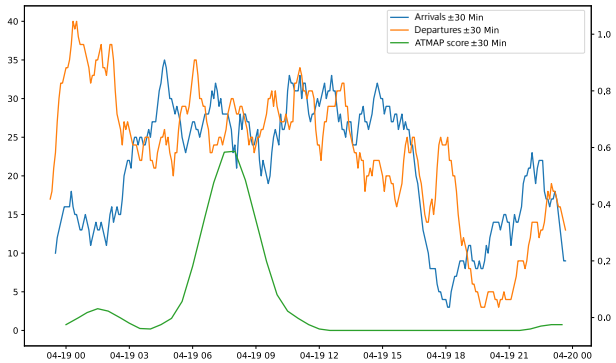

Figure 3. Combination of the air traffic diagrams of the arriving and departing flights flights incl. ATMAP score and operating direction.

inflating peaks. The resulting profile reproduces the "main cloud" in the arrivals–departures around approximately 20 to 30 movements per rolling hour in the high-utilization part of the day, together with the predictable evening reduction. Because the source days are direction-stable, dispersion around the curve is small (narrow interquartile bands), giving a tight and operationally credible envelope. We adopt $U_{\mathrm{ref}}^{\mathrm{N}}(t)$ as the North-ops reference plateau; in the next step we will quantify the depth and duration of capacity deltas on flip days by contrasting realized rolling counts with this reference, thereby parameterizing the depressions that a runway-aware arrival management optimizer must anticipate and bridge.

Figure 4 sketches the typical evolution of realized movements around a direction change. Starting from the steady baseline (dashed line), controllers typically "squeeze" the

last slots in the outgoing configuration, creating a modest last-minute rush whose amplitude c^+ measures the peak overshoot above baseline and whose duration t^+ covers the brief build-up window before the switch. Once the flip is initiated, sequencing is re-built, STARs are swapped, and departures are re-ordered; the system enters a constrained regime with a pronounced capacity drop of depth c^- below baseline that persists for t^-. This is the interval in which pushing demand risks stacking arrivals against a weakened terminal system. As the new configuration stabilizes and the backlog accumulated during t^- is released, throughput briefly exceeds the baseline again—the opening rush—characterized by an overshoot c^{++} sustained over t^{++} before the process relaxes back to the nominal envelope. In practice, c^+ and t^+ are small and asymmetric (a gentle pre-flip ramp), c^- and t^- set the dominant constraint (deeper and longer when flips cluster), and c^{++} , t^{++} appear when pent-up demand is available (e.g., mid-day). The tuple $\{(c^+, t^+), (c^-, t^-), (c^{++},t^{++})\}$ thus provides a compact, runway-aware parameterization that can be superimposed on the Normal-ops template and used directly as the capacity envelope for LR-ATFM optimization.

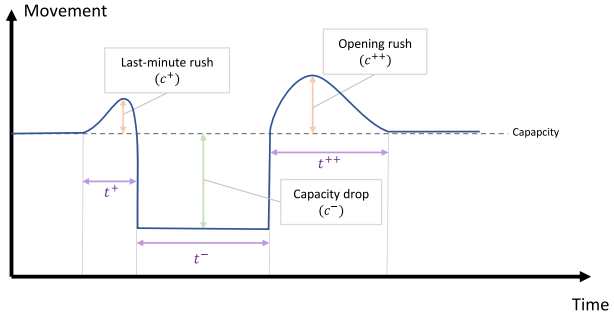

Figure 4. Schematic runway-flip response (rolling-hour movements).

To quantify weather-driven capacity variability, we compared a random day (25 September) rolling-hour entries (ten operating-direction transitions) against the Normal-ops template. Three repeatable signatures emerged. First, a reduction of throughput begins about 10–15 min before a flip. Second, each change is followed by a transient trough whose depth and duration depend on the time of day: in the early-morning cluster (04:30–06:30) the average deficit in the first 30 min after the flip reached -8 to -15 movements/h, and the depressed state persisted 45–60 min, extending to 90 min when flips occurred back-to-back. By contrast, mid-morning flips produced milder drawdowns (-3 to -6/h for 30-45 min). Third, re-stabilization often yields a short compensating bump: at 11:20 and 12:10 the realized counts exceeded the reference by +2 to +4/h for 20–30 min as the sequence was re-built.

Outside these flip windows, throughput closely tracked the stable reference — 21–24/h through the morning, 26–27/h near midday, and the routine evening trough (3–7/h). As can be seen in Figure 5, these observations motivate a simple runway-aware capacity model: a reference curve from stable North-ops, modulated by 15-min pre-ramp notches of time-of-day-dependent depth (5/h typical; 10–15/h for early-morning flips), 45–60 min post-flip duration (longer if flips are consecutive), and, for midday cases, a brief +2 to +4/h compensation bump. This piecewise envelope is the reference against which the LR-ATFM optimization is evaluated.

B. Mathematical model

In this section, we present the mathematical optimization framework that determines the most suitable set of flight options to minimize total overload across the entire planning horizon.

Sets:

T	discrete set of time periods within the optimization horizon
I	index set of all flights
J_i	feasible options for flight i

Parameters:

U_t	nominal approach sector capacity (depending on time t)
M	a sufficiently large penalty coefficient
T_{ijt}	binary constant, equal to 1 if option j of flight i is in the sector at time t, 0 otherwise

Decision variables:

x_{ij}	binary variable, equals 1 if option j of flight i is chosen, 0 otherwise
ρ_t	nonnegative integer variable, representing the excess demand over capacity at time t

$$min \sum_{t \in T} M\, \rho_t \tag{2}$$

s.t.

$$\sum_{i \in I} \sum_{j \in J_i} x_{ij}\, T_{ijt} - \rho_t \leq U_t \qquad \forall t \in T \tag{3}$$

$$\sum_{j \in J_i} x_{ij} = 1 \qquad \forall i \in I \tag{4}$$

$$x_{ij} \in \{0,1\}, \rho_t \in \{0,1,...,\infty\} \qquad \forall i \in I,\, j \in J_i,\, t \in T \tag{5}$$

The optimization problem in Equation (2) seeks to minimize the total overload during the optimization horizon. It minimizes the penalties of any violation of sector capacity with weight M. Constraint (3) enforces that the number of flights in the approach sector at time t does not exceed the available capacity (U_t). If infeasibility arises, the slack variable ρ_t allows controlled relaxation, indicating how many flights exceed the nominal capacity. Constraint (4) ensures that each flight i must be assigned exactly one option. Finally, Constraint (5) defines the domains of the decision variables.

Using the runway-aware capacity profile U_t for 25 September (Figure 6), we solved the sector-entry metering problem with discrete, LR-ATFM-feasible time-shift options, using Gurobi Solver. The optimized schedule (green) reduces the area of capacity exceedance from 2085 to 395 flight-minutes (-81%), largely removing the morning and mid-day overloads highlighted by the orange shading. Remaining violations are short and confined to the severe double-flip window around 05:30-06:30, where the capacity trough is both deep and brief and the maximum residual exceedance is 6 aircraft at 06:45.

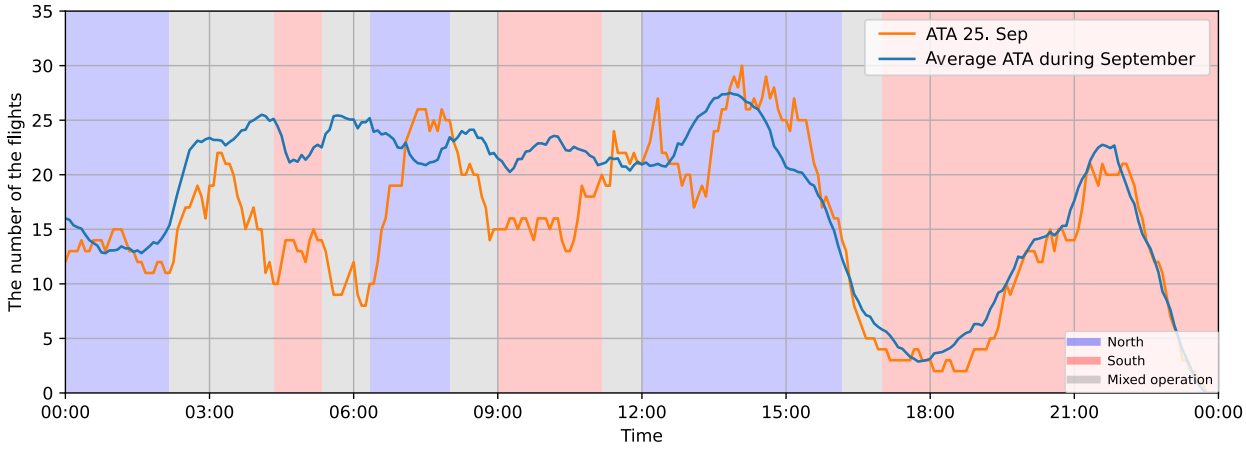

Figure 5. Throughput impacts of runway changes on 25 Sep vs. Normal-ops reference based on the actual time oarrival.

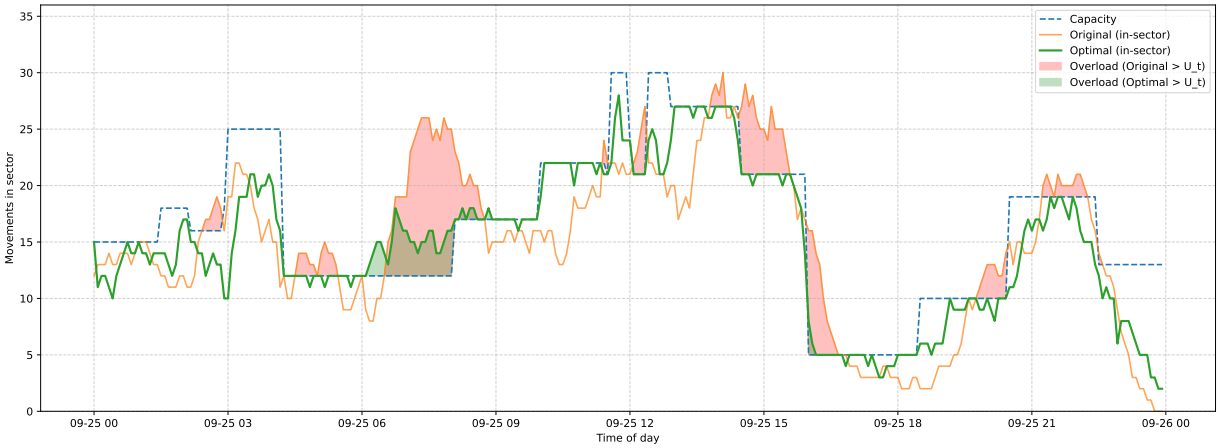

Figure 6. Runway-aware metering on 25 Sep: time-varying capacity (dashed), original sector entries (orange), optimized entries (green).

Outside this cluster, demand is re-phased toward the pre-flip rush and post-stablization opening shoulder, keeping the optimized trajectory close to, but generally below, the capacity (U_t) while preserving the afternoon plateau and evening build-up. In total, the flights are assigned feasible options, with most adjustments modest in magnitude—consistent with practical in-cruise speed advisories under LR-ATFM.

V. Conclusion

We presented an empirically grounded, runway-aware LR-ATFM framework for WSSS that converts weather and operating-direction dynamics into actionable capacity guidance for upstream metering. Three contributions stand out. First, we derived a direction-specific Normal-ops template from a flip-free block (5-20 Sep 2019), anchoring capacity around the observed "main cloud" of 20–30 movements per rolling hour and preserving the routine evening trough. Second, we quantified the typical flip response through a compact tuple that captures the pre-flip soft ramp, the post-flip drawdown and its persistence, and the short re-stabilization bump. On 25 Sep 2019, the drop begins 10–15 minutes before a change; early-morning clusters yield the deepest, longest troughs, whereas mid-day flips are shorter and shallower. Third, we embedded this piecewise envelope in a sector-entry metering model consistent with LR-ATFM operations at a 170-NM reference, demonstrating an 81% reduction in the area of overload (from 2085 to 395 flight-minutes) while keeping residual exceedances brief and localized to the most severe flip window.

Operationally, the results argue against regulating demand to a static ceiling. Instead, pushing entries against a time-indexed, runway-aware envelope allows pre-tactical steering around anticipated troughs and better exploitation of opening shoulders after re-stabilization. The approach is lightweight and portable: it relies on routine METAR, simple track filters near the airport, and rolling-hour counts, and it interfaces naturally with AMAN. As further steps, our capacity envelope is deterministic and conditioned on ex-post flips; coupling it with probabilistic flip forecasts (e.g., NWP-driven (Numerical Weather Prediction) wind-component predictions fused with ATMAP trends), or with advanced decision-support systems that can provide accurate airport runway configurations forecast hours in advance [32], would enable robust metering.

Airline-centric costs, equity constraints, and multi-airport

interactions along dominant flows warrant explicit treatment. Finally, LR-ATFM targets with AMAN revisions—offers a path to operational deployment. Even with these caveats, the evidence is clear: modest, well-timed upstream adjustments, informed by runway-aware capacity, can substantially de-risk peak periods at a weather-sensitive hub.

Disclosure

References

[1] Y. Chen, Y. Zhao, F. Fei, and H. Yang, "Optimizing large-scale demand and capacity balancing in air traffic flow management using deep neural networks," *Aerospace*, vol. 11, no. 12, p. 966, 2024.

[2] M. Schultz, D. Lubig, E. Asadi, J. Rosenow, E. Itoh, S. Athota, and V. N. Duong, "Implementation of a long-range air traffic flow management for the asia-pacific region," *IEEE Access*, vol. 9, pp. 124 640–124 659, 2021.

[3] E. Itoh, K. Tominaga, M. Schultz, and V. N. Duong, "Untangling complexity in asean air traffic management through time-varying queuing models," *Aerospace*, vol. 11, no. 1, p. 11, 2023.

[4] G. Enea, A. Andreeva-Mori, J. Bronsvoort, J. Hochwarth, T. Reynolds, and Onji, "Implementation of long-range air traffic flow management at large hub airports: An international perspective," in *Proceedings of the 15th USA/Europe Air Traffic Management (ATM) R&D Seminar*, 2023.

[5] L. Huang, S. Zhang, Y. Zhang, Y. Zhang, and Y. Yin, "Aircraft landing time prediction with deep learning on trajectory images," *arXiv preprint arXiv:2401.01083*, 2024.

[6] D. Kulkarni, "Models of maximum flows in airspace sectors in the presence of multiple constraints," in *2017 IEEE/AIAA 36th Digital Avionics Systems Conference (DASC)*. IEEE, 2017, pp. 1–8.

[7] J. Rosenow, E. Asadi, D. Lubig, M. Schultz, and H. Fricke, "Long range air traffic flow management with flight-specific flight performance," *Future Transportation*, vol. 2, no. 2, pp. 310–327, 2022.

[8] Airport Technology, "Changi international airport, singapore," Airport Technology, Jan. 2024, accessed: 2025-09-26. [Online]. Available: https://www.airport-technology.com/projects/changi-international-airport-singapore/

[9] D. C. Tascón and O. D. Olariaga, "Air traffic forecast and its impact on runway capacity. a system dynamics approach," *Journal of Air Transport Management*, vol. 90, p. 101946, 2021.

[10] A. Khattak, P.-w. Chan, F. Chen, and H. Peng, "Assessing wind field characteristics along the airport runway glide slope: An explainable boosting machine-assisted wind tunnel study," *Scientific Reports*, vol. 13, no. 1, p. 10939, 2023.

[11] Y. Tee and Z. W. Zhong, "Modelling and simulation studies of the runway capacity of changi airport," *The Aeronautical Journal*, vol. 122, no. 1253, pp. 1022–1037, 2018.

[12] A. Barea, R. de Celis, and L. Cadarso, "Integration of airport terminal arrival route selection, runway assignment and aircraft trajectory optimisation," *Transportation Research Procedia*, vol. 47, pp. 299–306, 2020.

[13] P. Sengupta, M. D. Tandale, and P. K. Menon, "Risk-hedged traffic flow management under airspace capacity uncertainties," *Journal of Guidance, Control, and Dynamics*, vol. 37, no. 5, pp. 1487–1500, 2014.

[14] D. Pham, M. Ngo, N. Tran, S. Alam, and V. Duong, "Changi airport," in *Air Traffic Management and Systems IV: Selected Papers of the 6th ENRI International Workshop on ATM/CNS (EIWAC2019)*, vol. 731. Springer Nature, 2021, p. 113.

[15] M. Schultz, S. Lorenz, R. Schmitz, and L. Delgado, "Weather Impact on Airport Performance," *Aerospace*, vol. 5, no. 4, p. 109, 2018.

[16] D.-M. C. Hartmann, *Meteorologische Einflüsse auf die Flugphase eines Luftfahrzeuges*. Deutscher Wetterdienst, Vorhersage- und Beratungszentrale Offenbach, 2016.

[17] Eurocontrol, "Algorithm to describe weather conditions at European airports," 2011.

[18] R. R. Pacheco, E. Fernandes, and E. M. Domingos, "Airport airside safety index," *Journal of Air Transport Management*, vol. 34, pp. 86–92, 2014.

[19] B. Wang, J. Liu, H.-J. Kim, P. J. Webster, and S.-Y. Yim, "Recent change of the global monsoon precipitation (1979–2008)," *Climate Dynamics*, vol. 39, no. 5, pp. 1123–1135, 2012.

[20] C.-P. Chang, Z. Wang, J. McBride, and C.-H. Liu, "Annual cycle of southeast asia—maritime continent rainfall and the asymmetric monsoon transition," *Journal of climate*, vol. 18, no. 2, pp. 287–301, 2005.

[21] B. M. Tan, *Changi Airport*. National Library Board (NLB), 2016.

[22] Airport Technology. (2024, Jan.) Changi international airport, singapore. Accessed: 2025-09-26. [Online]. Available: https://www.airport-technology.com/projects/changi-international-airport-singapore/

[23] Changi Airport Group. (2025, May) Fact sheet: Changi airport. Accessed: 2025-09-26. [Online]. Available: https://www.changiairport.com/en/corporate/our-media-hub/newsroom/press-releases.fact-sheet-changiairport.2025.all.html

[24] E. Choi and A. Tanurdjaja, "Extreme wind studies in singapore: An area with mixed weather system," *Journal of Wind Engineering and Industrial Aerodynamics*, vol. 90, no. 12-15, pp. 1611–1630, 2002.

[25] "Observed climate change over singapore," 2021.

[26] P. Clift, "The asian monsoon: causes, history and effects," 2008.

[27] X. Li, A. Meshgi, and V. Babovic, "Spatio-temporal variation of wet and dry spell characteristics of tropical precipitation in singapore and its association with enso," *International Journal of Climatology*, vol. 36, no. 15, pp. 4831–4846, 2016.

[28] J. M. Levine, "Constraining dark photon dark matter with the dark e-field radio experiment," Ph.D. dissertation, University of California, Davis, 2025.

[29] M. Schultz, D. Lubig, J. Rosenow, E. Itoh, S. Athota, and V. N. Duong, "Concept of a long-range air traffic flow management," in *EUROCONTROL SESAR Innovation Days*, 2020.

[30] V. Aditya, D. S. Aswin, S. V. Dhaneesh, S. Chakravarthy, B. S. Kumar, and M. Venkadavarahan, "A review on air traffic flow management optimization: trends, challenges, and future directions," *Discover Sustainability*, vol. 5, no. 1, p. 519, 2024.

[31] S. Liu, J. Zhang, Z. Peng, H. Guo, and A. Pi, "Identifying operational benefits of the arrival management system–a kpi-based experimental method by evaluating radar trajectories," *Promet-Traffic&Transportation*, vol. 33, no. 5, pp. 633–645, 2021.

[32] T. Reynolds, M. Matthews, D. Clark, S. Splawinski, K. Arnold, and M. Williams, "Weather considerations for airport capacity decision support development," in *Proceedings of the 16th USA/Europe Air Traffic Management (ATM) R&D Seminar*, 2025.